6-Substituted Quinolines as RORγt Inverse Agonists

J. Kent Barbay, Maxwell D. Cummings, Marta Abad, Glenda Castro, Kevin D. Kreutter, David A. Kummer, Umar Maharoof, Cynthia Milligan, Rachel Nishimura, Joan Pierce, Celine Schalk-Hihi, John Spurlino, Virginia M. Tanis, Maud Urbanski, Hariharan Venkatesan, Aihua Wang, Craig Woods, Ronald Wolin, Xiaohua Xue, James P. Edwards, Anne M. Fourie, Kristi Leonard

PII: S0960-894X(17)31012-0
DOI: https://doi.org/10.1016/j.bmcl.2017.10.027
Reference: BMCL 25356

To appear in: *Bioorganic & Medicinal Chemistry Letters*

Received Date: 12 June 2017
Revised Date: 12 October 2017
Accepted Date: 14 October 2017

Please cite this article as: Barbay, J.K., Cummings, M.D., Abad, M., Castro, G., Kreutter, K.D., Kummer, D.A., Maharoof, U., Milligan, C., Nishimura, R., Pierce, J., Schalk-Hihi, C., Spurlino, J., Tanis, V.M., Urbanski, M., Venkatesan, H., Wang, A., Woods, C., Wolin, R., Xue, X., Edwards, J.P., Fourie, A.M., Leonard, K., 6-Substituted Quinolines as RORγt Inverse Agonists, *Bioorganic & Medicinal Chemistry Letters* (2017), doi: https://doi.org/10.1016/j.bmcl.2017.10.027

6-Substituted Quinolines as RORγt Inverse Agonists

Authors: J. Kent Barbay*[,c], Maxwell D. Cummings*[,b], Marta Abad[b], Glenda Castro[a], Kevin D. Kreutter[c], David A. Kummer[a], Umar Maharoof[c], Cynthia Milligan[b], Rachel Nishimura[a], Joan Pierce[a], Celine Schalk-Hihi[b], John Spurlino[b], Virginia M. Tanis[a], Maud Urbanski[c], Hariharan Venkatesan[a], Aihua Wang[c], Craig Woods[a], Ronald Wolin[a], Xiaohua Xue[a], James P. Edwards[a], Anne M. Fourie[a], Kristi Leonard[c]

Corresponding Authors: kbarbay@its.jnj.com (J. K. Barbay), mcummin1@its.jnj.com (M. D. Cummings)

Addresses:

[a]*Discovery Immunology, Janssen Research and Development, LLC, 3210 Merryfield Row, San Diego, CA 92121*
[b]*Discovery Sciences, Janssen Research and Development, LLC, Welsh and McKean Roads, Spring House, PA 19477*
[c]*Discovery Immunology, Janssen Research and Development, LLC, Welsh and McKean Roads, Spring House, PA 19477*

Keywords. RORγt, retinoic acid-related orphan nuclear receptor gamma t, Th17, IL-17

Abstract: We identified 6-substituted quinolines as modulators of the retinoic acid receptor-related orphan receptor gamma t (RORγt). The synthesis of this class of RORγt modulators is reported, and optimization of the substituents at the quinoline 6-position that produced compounds with high affinity for the receptor is detailed. This effort identified molecules that act as potent, full inverse agonists in a RORγt-driven cell-based reporter assay. The X-ray crystal structures of two full inverse agonists from this chemical series bound to the RORγt ligand binding domain are disclosed, and we highlight the interaction of a hydrogen-bond

acceptor on the 6-position substituent of the inverse agonist with Glu379:NH as a conserved binding contact.

Retinoic acid receptor-related orphan receptor gamma t (RORγt) is a nuclear hormone receptor expressed in a variety of cell types of the innate and adaptive immune system.[1] This transcription factor drives Th17 cell differentiation and the production of cytokines including interleukin (IL)-17A and IL-17F.[2] Th17 cells and IL-17 have been shown to play an important role in the development of autoimmune disorders including psoriasis, multiple sclerosis, rheumatoid arthritis, Crohn's disease, and systemic lupus erythematosus.[3] RORγt-deficient mice show significantly reduced Th17 cell populations and decreased susceptibility to experimental autoimmune encephalomyelitis as well as intestinal and skin inflammation.[1,4] Clinical efficacy with biologics targeting IL-17A, or IL-23, the cytokine that stabilizes Th17 cells, in psoriasis and psoriatic arthritis has served to validate the critical role of IL-17A, IL-23 and Th17 cells in these autoimmune diseases.[5] Targeting RORγt, the key regulator in the Th17/IL-17 pathway, provides a novel opportunity to treat autoimmune diseases with a small molecule drug. RORγt contains a ligand binding domain (LBD) capable of binding small molecules that influence interactions with co-activator and co-repressor proteins and thereby modulate gene transcription. Many recent reports have detailed the development of RORγt modulators.[6-9]

We conducted a high-throughput screen to identify RORγt modulators using ThermoFluor®, a fluorescence-based, thermal shift assay.[10] Among compounds found to bind to the LBD of RORγt was quinoline **1** (K_d 160 nM). The HTS sample was a racemate that displayed full inverse agonism in a RORγt driven cell-based (1-hybrid) reporter assay (IC_{50} 260

nM, 101% inhibition at 6 μM).[11] Structure-activity relationships (SAR) and variations in the mechanism of action (agonists, inverse agonists, and neutral antagonists) established during optimization of the substituents at the 2-, 3-, and 4-positions on the quinoline core have been described.[12] Herein, we report the synthesis of compounds with changes to the substituents on the carbon bearing the tertiary alcohol group of **1** that led to a series of full inverse agonists with improved potency. We also describe co-crystal structures of two ligands bound to the RORγt ligand binding domain that provide structural insights into the SAR discussed in this paper.

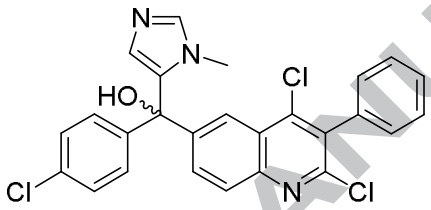

1
Binding K_d 160 nM
Cell reporter IC_{50} 260 nM

Figure 1. Structure of high-throughput screening hit **1**.

Initially, the two aryl groups attached to the carbon atom bearing the tertiary alcohol were explored while retaining the other structural features of the screening hit. In our initial exploratory hit-to-lead studies, the early compounds in this series (Table 1) were tested as racemic mixtures, while more potent analogs prepared later were resolved into single enantiomers as detailed below. 1,2-Dimethyl imidazole **2** retained comparable binding affinity to that of **1**, while expansion of the *N*-methyl substituent to *N*-ethyl led to decreased affinity (**3**, K_d 450 nM). A series of pyridines paired with the *N*-methyl imidazole group was also explored. Both 4-pyridyl (**4**, K_d 14 nM) and 3-pyridyl analogs (**5**, K_d 38 nM) displayed improved binding affinity and activity in the 1-hybrid cell-based reporter assay (IC_{50}'s 50 nM and 140 nM,

respectively). These compounds showed considerably stronger binding affinities than the corresponding 2-pyridyl analog (**6**, 960 nM).

Consistent with a specific intermolecular interaction, binding affinity and cellular potency were sensitive to hydrogen bond acceptor position in the aryl substituents on the carbon bearing the tertiary alcohol. For example, 1-methyl-imidazol-5-yl analog **7** displayed 5 nM affinity for the receptor and an IC_{50} of 21 nM in the 1-hybrid assay, whereas the 1-methyl-imidazol-2-yl isomer **8**, with the imidazole nitrogen shifted by one position, showed a 4,000-fold reduction in binding affinity (K_d 20,000 nM). Similarly, the 3-pyridyl analog **9** displayed a binding affinity of 76 nM and an IC_{50} of 130 nM in the cell assay, while the corresponding 4-pyridyl analog **10** displayed 20-fold weaker affinity and a corresponding reduction in cell potency (Table 1).

Compounds **11**-**15** represent a series of analogs in which one of the aryl groups is fixed as 1-methyl-imidazol-5-yl. High levels of potency were achieved by incorporation of *ortho*-substituted 4- or 3-pyridyls, e.g. *m*-methyl-4-pyridyl inverse agonist **11**, which had a K_d of 0.6 nM and 1-hybrid assay IC_{50} of 13 nM. The protein is also able to accommodate larger fused aryls in this position, as indicated by quinoline **14** (K_d 0.5 nM, 1-hybrid IC_{50} 5.5 nM), as well as 5-membered heterocycles, as exemplified by thiazole **15** (K_d 1.1 nM, 1-hybrid IC_{50} 100 nM).

Table 1. Binding and cell-based functional data of 3-phenyl-2,4-dichloroquinolines.[a]

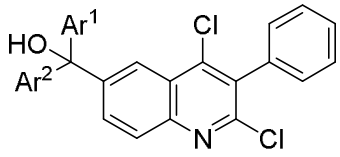

Cmpd #	Ar^1	Ar^2	ThermoFluor® binding to RORγt LBD, K_d (nM)	RORγt cell-based reporter assay IC_{50} (nM) (% inhibition at 6 μM)
1	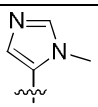	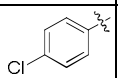	160	260 (101)
2	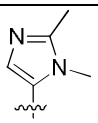	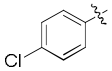	190	600 (106)
3	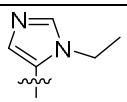	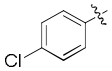	450	820 (101)
4		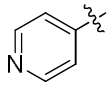	14	50 (105)
5		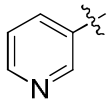	38	140 (103)
6	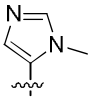	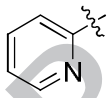	960	1000 (93)
7	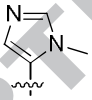	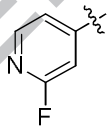	5.3	21 (103)
8		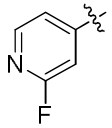	20000	>6,000 (37)
9	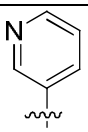	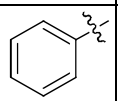	76	130 (100)
10	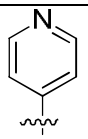	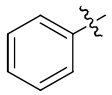	1500	2100 (84)
11	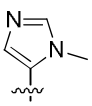	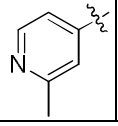	0.60	13 (104)

12	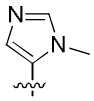	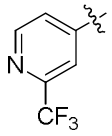	6.4	82 (101)
13	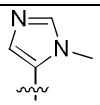	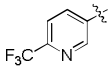	31	180 (100)
14	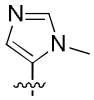	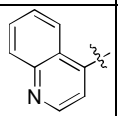	0.50	5.5 (101)
15	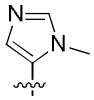	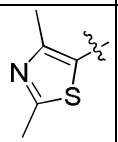	1.1	100 (104)

[a] Compounds in Table 1 were tested as racemic mixtures.

Screening hit **1** was separated into individual enantiomers **1a** and **1b** by chiral chromatography. The enantiomers exhibited a 180-fold difference in binding affinity (32 nM vs 5700 nM, respectively, Table 2). This result is consistent with receptor modulation by a specific ligand/receptor interaction and emphasizes the importance of an optimally positioned hydrogen-bond acceptor in at least one of the aryl groups flanking the tertiary alcohol (e.g., the 3-position nitrogen of the imidazole in only one of the enantiomers of **1**).

Table 2. Activities of single enantiomers of screening hit **1**.

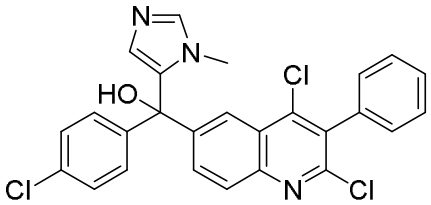

Cmpd #	ThermoFluor® binding to RORγt LBD, K_d (nM)	RORγt cell-based reporter assay IC_{50} (nM) (% inhibition at 6 μM)
1[a]	160	260 (101)
1a[b]	32	220 (100)
1b[b]	5700	~5500 (58)

[a] Racemate.
[b] Single enantiomer, absolute stereochemistry not determined.

Subsequent racemic mixtures were separated by chiral chromatography to provide single enantiomers for additional SAR exploration in this series. This work was carried out on the 2-methoxy-3-(1-pyrazole-benzyl)-4-chloro scaffold and is detailed in Table 3. In cases where only one enantiomer is presented in Table 3, it is the more potent isomer with regard to binding to the RORγt LBD as measured in the ThermoFluor® assay. The 2-methoxy group was introduced to remove potential chemical reactivity associated with 2-chloroquinolines, and a substituted benzyl group at the 3-position yielded potent, full inverse agonists.[12] As previously noted, large differences in the binding potencies of enantiomers were sometimes observed. For example, in this series, compound **16a** (K_d 9.2 nM) bearing the original aryl substituents (1-methylimidazol-5-yl and *p*-chlorophenyl) was 57-fold more potent than the less active enantiomer **16b**. Analogs **17** and **18** explored the impact of replacing the tertiary alcohol with amino and methylamino groups, respectively. Replacement of the alcohol with an amino group resulted in an approximately 12-fold decrease in binding affinity (K_d 110 nM), and *N*-methylation of the amino group further reduced binding (K_d 280 nM). The *ortho*-trifluoromethyl 3-pyridyl enantiomers **19a** and **19b** delivered strong potency, with a more modest difference in potency seen between

enantiomers (14-fold). Returning to combinations of two 5-membered heterocycles yielded potent enantiomers **20a** and **20b**, with 1,2-dimethylimidazole and *N*-methyltriazole groups flanking the tertiary alcohol. These cases illustrate that systems in which both heteroaryls have a suitably positioned hydrogen bond acceptor can yield highly potent compounds for both enantiomers. The observation that both enantiomers **20a** and **20b** were active suggested to us that exploration of symmetrical, achiral compounds bearing two identical 5-membered heterocycles might be productive. To test this, achiral molecules bis-1-methyltriazole **21** and bis-1,2-dimethylimidazole **22** were synthesized, and, as expected, they demonstrated high binding affinities (K_d 5.0 nM and 0.27 nM, respectively). Interestingly, both enantiomers of secondary alcohols **23a** and **23b** also bound to the receptor with approximately equal potency (K_d's 69-91 nM), in contrast to other examples of enantiomeric pairs containing only one H-bond acceptor (e.g. **1a/b** and **16a/b**). This may reflect a somewhat different binding mode or plasticity in the receptor pocket when a ring is removed, and indicates the potential for development of potent analogs with reduced molecular weights.

Compound **24a** incorporates an *N*-acetyl-piperidine group as replacement for one of the aryl groups and retains potent binding affinity (K_d 20 nM) and cellular activity (1-hybrid IC_{50} 46 nM). The enantiomer, **24b**, retains high potency and reflects the ability of the *N*-acetyl group to act as an H-bond acceptor, as subsequently confirmed by X-ray crystallography (*vide supra*). By contrast, replacement of the *N*-acetylpiperidine ring with phenyl in compounds **25a** and **25b** again leads to a large divergence in the enantiomer potency (21-fold) in line with the SAR discussed above.

Table 3. Binding and cell-based functional data of 2-methoxy-3-(1-pyrazole-benzyl)-4-chloroquinolines.[a]

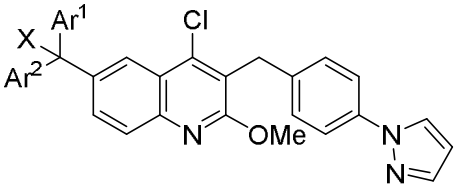

Cmpd #	Ar^1	Ar^2	X	ThermoFluor® binding to RORγt LBD, K_d (nM)	RORγt cell-based reporter assay IC_{50} (nM) (% inhibition at 6 μM)
16a		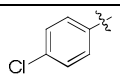	OH	9.2	73 (99)
16b		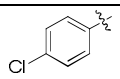	OH	520	670 (87)
17	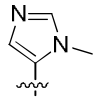	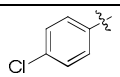	NH_2	110	210 (97)
18	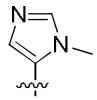	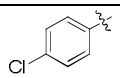	NHMe	280	630 (90)
19a	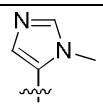	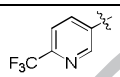	OH	5.0	89 (97)
19b	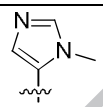	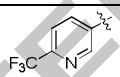	OH	70	170 (99)
20a	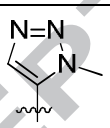	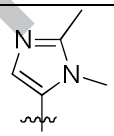	OH	1.2	13 (100)
20b	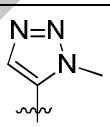	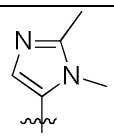	OH	0.38	5.3 (100)
21	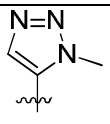	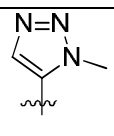	OH	5.0	6.6 (91)
22	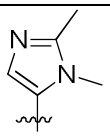	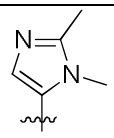	OH	0.27	200 (96)

23a	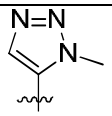	H	OH	69	270 (98)
23b	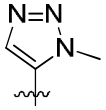	H	OH	91	300 (97)
24a	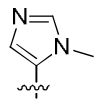	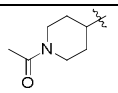	OH	20	46 (100)
24b	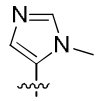	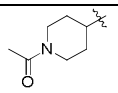	OH	33	59 (107)
25a	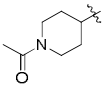	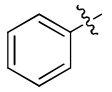	OH	3.6	24 (100)
25b	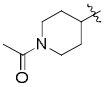	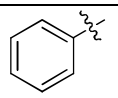	OH	77	140 (103)

[a] All chiral compounds are single enantiomers. Absolute stereochemistry is unknown unless specifically noted in the text.

Unlike changes previously described to the quinoline 3-position substituent,[12] compounds described in this paper uniformly displayed essentially full inverse agonism, as measured by percent inhibition of gene transcription in the 1-hybrid cell-based functional reporter assay at an inhibitor concentration of 6 μM. Except in cases of weak inverse agonists displaying potency in the μM range, ligands with varied substituents on the benzylic alcohol carbon displayed close to 100% inhibition at high ligand concentration.

Molecules in Tables 1-3 were prepared by the coupling of a diaryl ketone with a 6-lithioquinoline reagent, the latter formed initially by a halogen-lithium exchange reaction (Scheme 1).[13] 6-Bromo-2,4-dichloro-3-phenylquinoline **III** was prepared sequentially by acylation of 5-bromo-methyl 2-aminobenzoate **I** with 2-phenylacetyl chloride, lithium hexamethyldisilazane induced cyclization, and reaction of the resultant 4-hydroxyquinolinone

with phosphorus oxychloride. 2-Methoxy-3-(1-pyrazole-benzyl)-quinoline **IV**, used in the synthesis of compounds in Table 3, was prepared as previously described.[12] In the case of secondary alcohol inverse agonists (**23a/b**), ketone **V** was replaced with an aldehyde in the final step.[14]

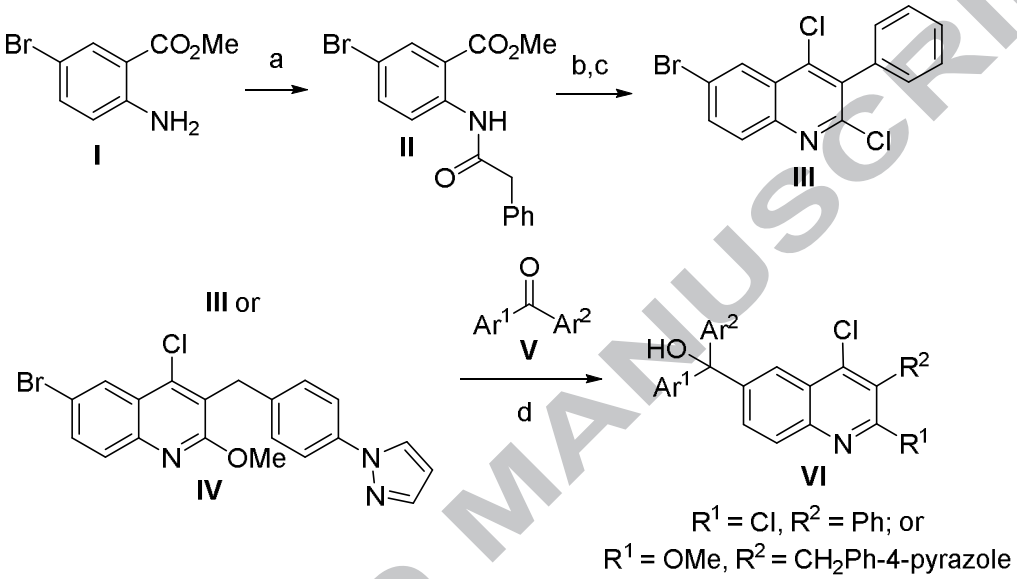

Scheme 1. (a) $PhCH_2COCl$, Et_3N, DCM; (b) LiHMDS, THF (c) $POCl_3$, reflux; (d) *n*-BuLi, THF.

The diaryl ketones used above were prepared by the general routes shown in Scheme 2. 5-Bromo-imidazoles **VII** were reacted with alkyl magnesium halides to generate Grignard reagents that were reacted with either a Weinreb amide to directly produce ketones **VIII** or with an aldehyde to produce a secondary alcohol which was then oxidized to the ketone. Symmetrical ketones were made by the reaction of heterocyclic anions with ethyl-*N*-(methoxy)-*N*-(methyl)carbamate, as illustrated in Scheme 2 for ketone **X**.[15]

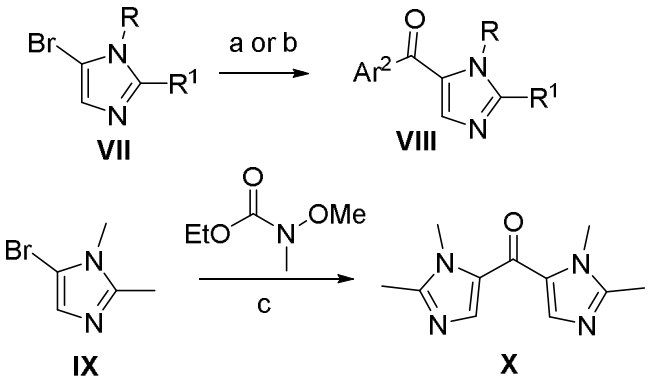

Scheme 2. (a) EtMgBr, THF; Ar^2-CONMe(OMe); (b) *i*-PrMgCl-LiCl, THF, Ar^2CHO; MnO_2, 1,4-dioxane, reflux; (c) *n*-BuLi, THF.

Compounds **17** and **18,** bearing amines at the benzylic position, were synthesized from the corresponding tertiary alcohol by acetylation of the alcohol and treatment with methanolic ammonia or methylamine (Scheme 3).

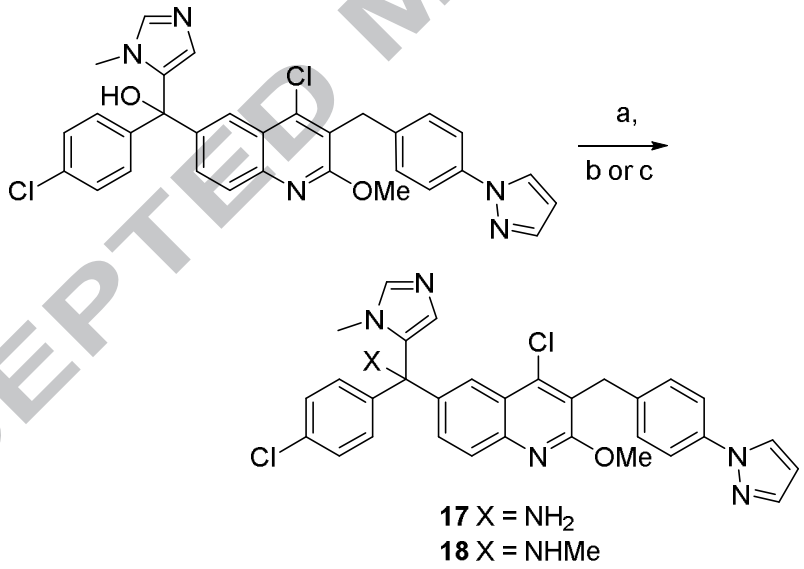

Scheme 3. (a) NaH, Ac_2O, DMF; (b) NH_3, MeOH; (c) CH_3NH_2, MeOH.

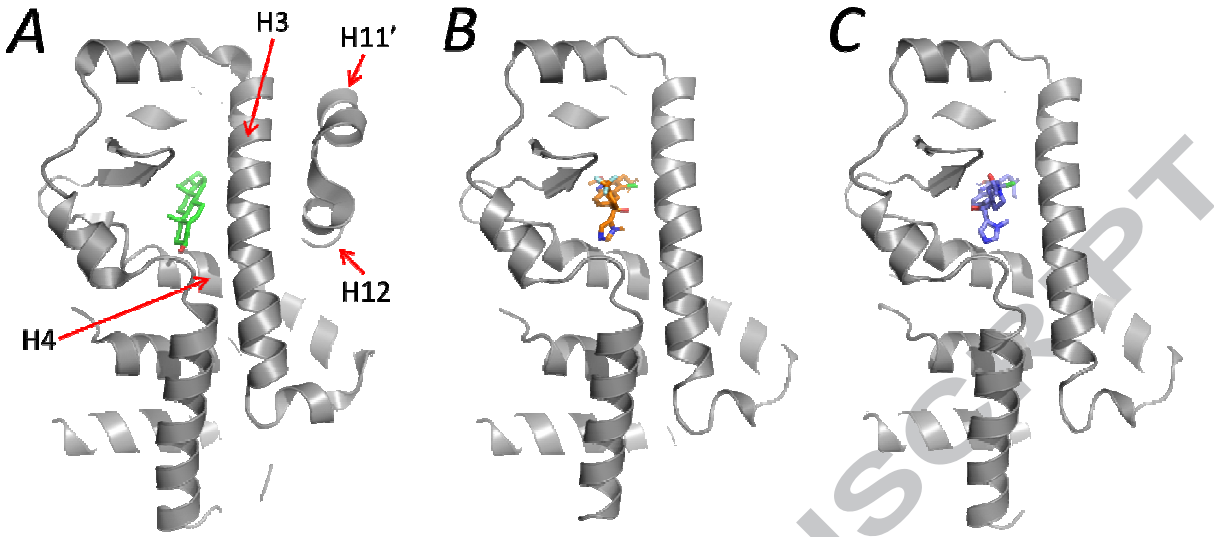

Figure 2. Crystal structures of RORγt ligand binding domain complexes. A-C: RORγt LBD, grey ribbon diagram; A: 25-hydroxycholesterol, green color-by-atom sticks (PDB ID: 3L0L)[16]; B: compound **19b**, orange color-by-atom sticks (PDB ID 5W4V); C: compound **24b**, purple color-by atom sticks (PDB ID 5W4R). Compounds **19b** and **24b** occupy the central 25-hydroxycholesterol binding pocket. Note the absence of H11' and H12 in B and C; binding of effectors of this and other chemotypes has been observed to lead to disorder in this region of the LBD.[12,17]

The crystal structure of **19b** bound to the LBD of human RORγt was determined at 3.0Å resolution. The absolute stereochemistry of **19b** was observed to be *R*, and, similar to our previous report on this chemical series,[12] the bound ligand occupies the buried and largely hydrophobic sterol binding pocket (Figure 2).[16,17] In our earlier report we focused on substituents at the 3-position of the quinoline core, while the present work addresses the tertiary alcohol and pendant rings of this quinoline chemotype.

In the observed binding mode, the 4-chloro-2-methoxyquinoline core of **19b** is positioned between the sidechains of Met365 and Phe378, forming an edge-to-face π-π interaction with the latter. The trifluoromethylpyridine ring is sandwiched between three aromatic sidechains, making a face-to-face contact with His323 and edge-to-face interactions with Phe377 and Phe378. The pyridine nitrogen accepts a hydrogen bond from the backbone amide of Glu379 (Figure 3). Modeling of a likely binding mode for **19a** indicates that a similar hydrogen bonding interaction is possible for the nitrogen of the *N*-methylimidazole of the other enantiomer (not shown), consistent with the high affinity observed for both enantiomers (**19a/b** in Table 3).

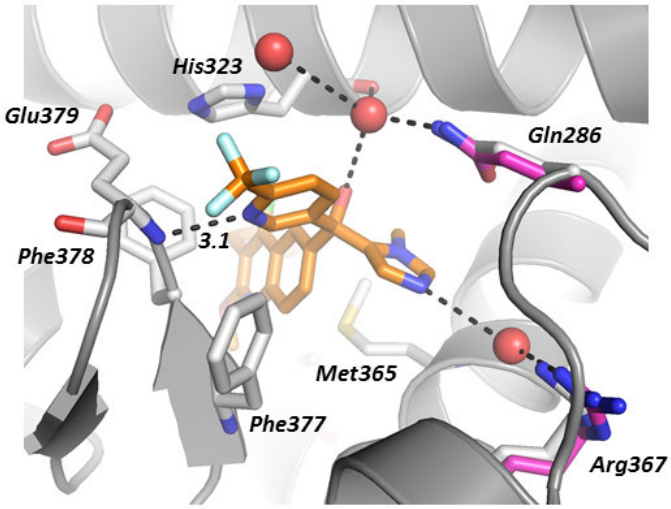

Figure 3. Crystal structure of compound **19b** bound to the RORγt ligand binding domain. RORγt LBD: grey ribbon and grey color-by-atom; compound **19b**: orange color-by-atom; bound water molecules (red spheres) are from the published 25-hydroxycholesterol complex structure,[16] and the sidechain conformations for Gln286 and Arg367 from this sterol complex are also shown (magenta color-by-atom) relative to the respective sidechains from the LBD-**19b** complex structure; selected residues are shown in stick format; the distance for one direct intermolecular

hydrogen bond is shown, in Å; selected contacts involving the modeled bound water molecules are indicated with dashed lines.

Comparison of the present structure with the published crystal structure of the 25-hydroxycholesterol agonist complex[18] offers some insight into the specific contribution of the tertiary hydroxyl group. Unlike the LBD-**19b** complex structure, bound water molecules are resolved in the higher resolution crystal structure of the sterol complex. Overlay of bound water molecules from the sterol complex onto the LBD-**19b** complex indicates that the ligand hydroxyl group may form part of a hydrogen bond network that involves bound water molecules as well as RORγt (Figure 3). Similar analysis suggests that the distal heteroatom of the *N*-methylimidazole may be forming a water-bridged intermolecular hydrogen bond with the guanidine of Arg367 (Figure 3). Both of these modeled bridging water contacts are consistent with the available structural information[19] as well as with the observed SAR for this chemotype (Table 3, Figure 3).

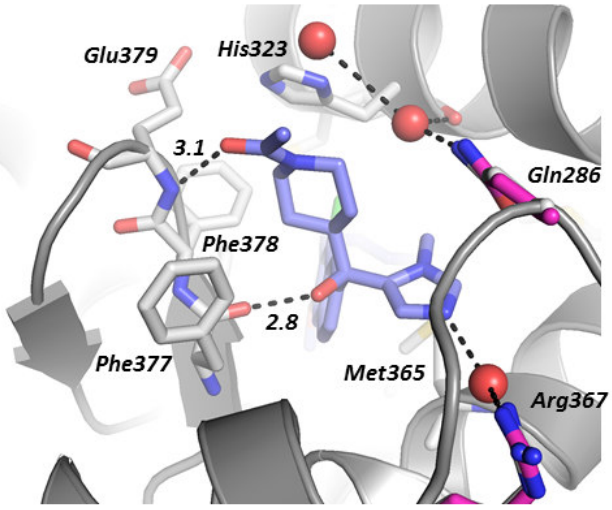

Figure 4. Crystal structure of compound **24b** bound to the RORγt ligand binding domain. RORγt LBD: grey ribbon and grey color-by-atom; compound **24b**: purple color-by-atom. As described for Figure 3, bound water molecules (red spheres) are from the published 25-hydroxycholesterol complex structure,[16] and the sidechain conformations for Gln286 and Arg367 from this sterol complex are also shown (magenta color-by-atom) relative to the respective sidechains from the LBD-**24b** complex structure; selected residues are shown in stick format; the distances for two direct intermolecular hydrogen bonds are shown, in Å; selected contacts involving the modeled bound water molecules are indicated with dashed lines.

The X-ray crystal structure of **24b** bound to the RORγt LBD was also determined to 3.0Å resolution. As for compound **19b** above, the *R*-enantiomer of **24b** was observed bound in this complex. The *N*-acetylpiperidine moiety of **24b** replaces the trifluoromethylpyridine of **19b**. The carbonyl of this acetyl group effectively mimics the pyridine nitrogen of **19b**, again forming an intermolecular hydrogen bond with the backbone amide of Glu379 (Figure 4). As previously determined for **19a** and **19b**, the corresponding enantiomer (**24a**) maintains high potency, further supporting the idea that the *N*-methylimidazole is able to engage in the same hydrogen bonding contact with the backbone of Glu379. The tertiary alcohol in this structure is rotated ~180° relative to the complex with **19b** (Figure 5), in this case forming a direct intermolecular hydrogen bond with the carbonyl oxygen of Phe377 (Figures 4 and 5). From more than a dozen protein-ligand complex structures that we have determined for this chemical series (not shown), the binding orientation for the hydroxyl group as seen in the complex with **19b** was observed

most frequently. Despite the reorientation of the hydroxyl group, the two rings attached at the benzylic carbon in **19b** and **24b** occupy similar regions of the receptor and the overall binding mode is conserved (Figures 3-5). We see that different functional groups from the two ligands (**19b** and **24b**) form an intermolecular hydrogen bond with the same Glu379:NH donor. It may be that this specific interaction drives the alternate orientation of the tertiary alcohol observed in the complex with **24b**. These structural observations, in conjunction with the SAR data presented above showing strong sensitivity of binding affinity to hydrogen bond acceptor atom placement in pendant rings at this position, suggest that the contact with Glu379:NH is an important interaction within this class of RORγt modulators.

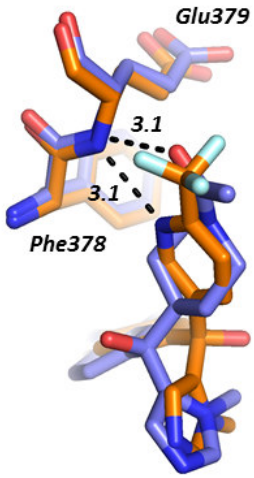

Figure 5. Superimposed RORγt binding conformations of **19b** and **24b**. **19b**: orange color-by-atom; **24b**: purple color-by-atom; Phe378 and Glu379 of the LBD from the corresponding crystal structures are shown, colored as **19b** and **24b**; distances shown, between the indicated ligand atoms and Glu379:N of the LBD from the relevant complex structure, are in Å. The overlay is based on superposition of the LBD in the crystal structures of the two complexes.

In summary, a high-throughput screen identified a series of 6-substituted quinolines that bind to RORγt. Optimization of groups flanking the tertiary alcohol at this position led to the discovery of compounds that bind to the receptor with high affinity and are full inverse agonists in a cell-based reporter assay. We have reported the co-crystal structures of two compounds with the RORγt ligand binding domain and described key interactions observed between potent inverse agonists and the receptor. Further characterization of compounds in this series will be described in additional reports.

Acknowledgment

Dr. Ulrike Hars (Crelux GmbH) determined the crystal structure of **19b** complexed to RORγt LBD.

References and Notes

1. Jetten, A. M. *Nucl. Recept. Signal.* **2009**, *7*, e003.

2. Ivanov, I. I.; McKenzie, B. S.; Zhou, L.; Tadokoro, C. E.; Lepelley, A.; Lafaille, J. J.; Cua, D. J.; Littman, D. R. *Cell* **2006**, *126*, 1121-1133.

3. Tabarkiewicz, J.; Pogoda, K.; Karczmarczyk, A.; Pozarowski, P.; Giannopoulos, K. *Arch. Immunol. Ther. Exp.* **2015**, *63*, 435-449.

4. (a) Withers, D. R.; Hepworth, M. R.; Wang, X.; Mackley, E. C.; Halford, E. E.; Dutton, E. E.; Marriott, C. L.; Brucklacher-Waldert, V.; Veldhoen, M.; Kelsen, J.; Baldassano, R. N.; Sonnenberg, G. F. *Nature Medicine* **2016**, *22*, 319-325. (b) Xue, X.; Soroosh, P.; De Leon-Tabaldo, A.; Luna-Roman, R.; Sablad, M.; Rozenkrants, N.; Yu, J.; Castro, G.; Banie, H.; Fung-Leung, W.-P.; Santamaria-Babi, L.; Schlueter, T.; Albers, M.; Leonard, K.; Budelsky, A. L.; Fourie, A. M. *Sci. Rep.* **2016**, *6*, 37977.

5. (a) Campa, M.; Mansouri, B.; Warren, R.; Menter, A. *Dermatol. Ther.* **2016**, *6*, 1-12. (b) Fragoulis, G. E.; Siebert, S.; McInnes, I. B. *Annu. Rev. Med.* **2016**, *67*, 27.1-27.17.

6. Kamenecka, T. M.; Lyda, B.; Chang, M. R.; Griffin, P. R. *Med. Chem. Commun.* **2013**, *4*, 764-776.

7. Solt, L. A.; Burris, T. P. *Trends Endocrin. Metabol.* **2012**, *23*, 619-627.

8. Solt, L.A.; Griffin, P. R.; Burris, T. P. *Curr. Opin. Lipidology* **2010**, *21*, 204-211.

9. Fauber, B. P.; Magnuson, S. *J. Med. Chem.* **2014**, *57*, 5871-5892.

10. (a) Pantoliano, M. W.; Petrella, E. C.; Kwasnoski, J. D.; Lobanov, V. S.; Myslik, J.; Graf, E.; Carver, T.; Asel, E.; Springer, B. A.; Lane, P.; and Salemme, F. R. *J. Biomol. Screen.* **2001**, *6*, 429-40. (b) Matulis, D.; Kranz, J. K.; Salemme, F. R.; Todd, M. J. *Biochemistry* **2005**, *44*, 5258-5266.

11. For assay details, see: Barbay, J. K.; Edwards, J. P.; Kreutter, K. D.; Kummer, D. A.; Maharoof, U.; Nishimura, R.; Urbanski, M.; Venkatesan, H.; Wang, A.; Wolin, R. L.; Woods, C. R.; Fourie, A.; Xue, X.; Cummings, M. D.; Leonard, K. A. *PCT Int. Appl.* WO 2015057203.

12. Kummer, D. A.; Cummings, M. D.; Abad, M.; Barbay, J.; Castro, G.; Wolin, R.; Kreutter, K. D.; Maharoof, U. M.; Milligan, C.; Nishimura, R.; Pierce, J.; Schalk-Hihi, C.; Spurlino, J.; Urbanski, M.; Venkatesan, H.; Wang, A.; Woods, C.; Xue, X.; Edwards, J. P.; Fourie, A. M.; Leonard, K. *Bioorg. Med. Chem. Lett.* **2017**, *27*, 2047-2057.

13. For additional synthetic details, see reference 11 and: Leonard, K. A.; Barbay, J. K.; Edwards, J. P.; Kreutter, K. D.; Kummer, D. A.; Maharoof, U.; Nishimura, R.; Urbanski, M.; Venkatesan, H.; Wang, A.; Wolin, R. L.; Woods, C. R.; Fourie, A.; Xue, X.; Cummings, M. D.; Jones, W. M.; Goldberg, S. *PCT Int. Appl.* WO 2015057205.

14. Leonard, K. A.; Barbay, K.; Edwards, J. P.; Kreutter, K. D.; Kummer, D. A.; Maharoof, U.; Nishimura, R.; Urbanski, M.; Venkatesan, H.; Wang, A.; Wolin, R. L.; Woods, C. R.; Fourie, A.; Xue, X.; Cummings, M. D. *PCT Int. Appl.* WO2015057206.

15. Hlasta, D. J.; Court, J. J. *Tet. Lett.* **1989**, *30*, 1773-1776.

16. Jin, L., Martynowski, D., Zheng, S., Wada, T., Xie, W., Li, Y. *Mol Endocrinol* **2010**, *24*, 923-929.

17. Part of helix 10/11 and all of helices 11' and 12 have been observed to be non-helical and/or disordered in crystal structures of effector-LBD complexes, including complexes with representatives from the present chemical series described in our earlier report (reference 12, and references therein). This structural observation seems generally consistent with effector mechanism, and has been observed with LBD protein constructs that include the complete LBD such as the 265-507 construct of our standard conditions (e.g. **24b**-RORγt LBD and structures in reference 12). The **19b**-RORγt LBD complex was generated under non-standard conditions involving treatment with V8 protease (*Staphylococcus aureus* endoproteinase Glu-C) that likely

led to truncation of the LBD C-terminus. In the **19b**-RORγt LBD complex structure reported here, the absence of H11' and H12 and the non-helicity of the observed C-terminus are likely explained by proteolytic cleavage at Glu481, near the H10/11 midpoint, rather than by a ligand-induced conformational change. However, the observed binding mode of **19b** is consistent with that of other members of this chemical series (e.g. **24b**, structures in reference 12, additional unpublished results), and the region of interest for the present analysis is at the opposite end of the binding site and does not include the (possibly) affected secondary structure elements.

18. At 3.0Å resolution we are unable to observe bound waters in the present structure, but they are observed in the higher resolution crystal structure of the agonist 25-hydroxycholesterol complexed with RORγ (reference 16).

19. The bound water nearest to the ligand hydroxyl is also observed in the digoxin complex structure: Fujita-Sato, S., Ito, S., Isobe, T., Ohyama, T., Wakabayashi, K., Morishita, K., Ando, O. Isono, F. *J. Biol. Chem.* **2011**, *286*, 31409-31417. Also, nearby sidechains that interact with two of the three bound waters displayed in Figures 3 and 4 maintain the same rotamers in the LBD-**19b** and LBD-**24b** complex structures as those observed in the published 25-hydroxycholesterol complex structure (reference 16).

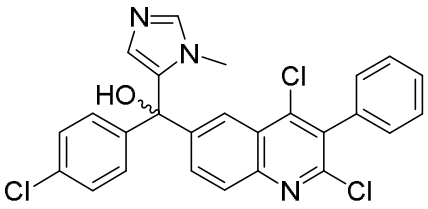

1

Binding K_d 160 nM

Cell reporter IC_{50} 260 nM

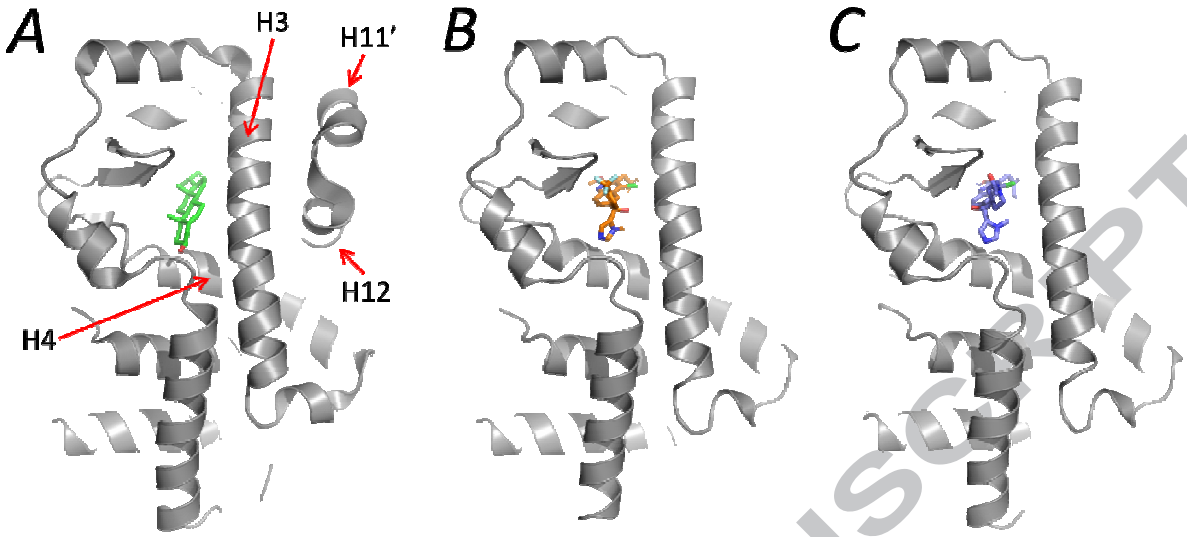

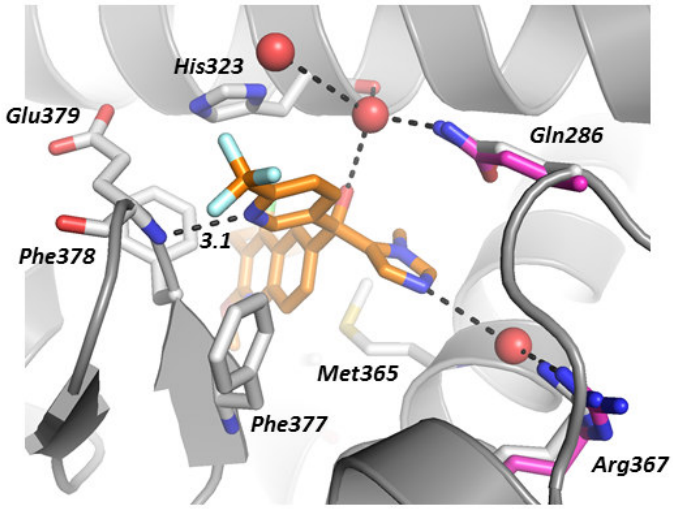

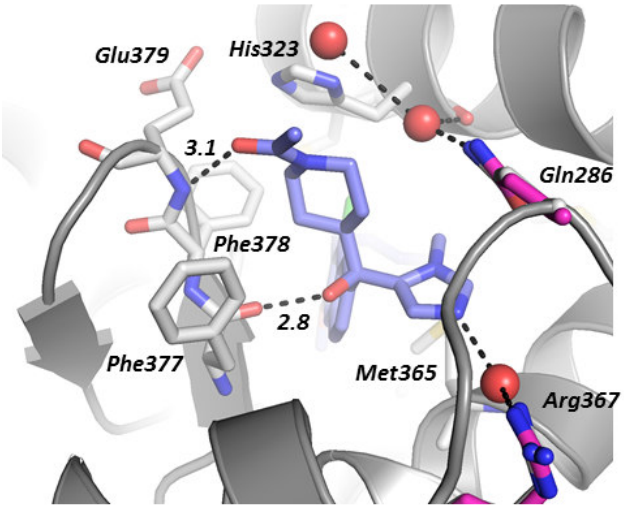

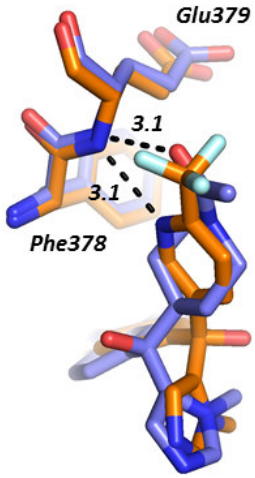

Figure 1. Structure of high-throughput screening hit **1**.

Figure 2. Crystal structures of RORγt ligand binding domain complexes. A-C: RORγt LBD, grey ribbon diagram; A: 25-hydroxycholesterol, green color-by-atom sticks (PDB ID: 3L0L)[16]; B: compound **19b**, orange color-by-atom sticks (PDB ID 5W4V); C: compound **24b**, purple color-by atom sticks (PDB ID 5W4R). Compounds **19b** and **24b** occupy the central 25-hydroxycholesterol binding pocket. Note the absence of H11' and H12 in B and C; binding of effectors of this and other chemotypes has been observed to lead to disorder in this region of the LBD.[12,17]

Figure 3. Crystal structure of compound **19b** bound to the RORγt ligand binding domain. RORγt LBD: grey ribbon and grey color-by-atom; compound **19b**: orange color-by-atom; bound water molecules (red spheres) are from the published 25-hydroxycholesterol complex structure,[16] and the sidechain conformations for Gln286 and Arg367 from this sterol complex are also shown (magenta color-by-atom) relative to the respective sidechains from the LBD-**19b** complex structure; selected residues are shown in stick format; the distance for one direct intermolecular hydrogen bond is shown, in Å; selected contacts involving the modeled bound water molecules are indicated with dashed lines.

Figure 4. Crystal structure of compound **24b** bound to the RORγt ligand binding domain. RORγt LBD: grey ribbon and grey color-by-atom; compound **24b**: purple color-by-atom. As described for Figure 3, bound water molecules (red spheres) are from the published 25-hydroxycholesterol complex structure,[16] and the sidechain conformations for Gln286 and Arg367 from this sterol complex are also shown (magenta color-by-atom) relative to the respective sidechains from the LBD-**24b** complex structure; selected residues are shown in stick format; the

distances for two direct intermolecular hydrogen bonds are shown, in Å; selected contacts involving the modeled bound water molecules are indicated with dashed lines.

Figure 5. Superimposed RORγt binding conformations of **19b** and **24b**. **19b**: orange color-by-atom; **24b**: purple color-by-atom; Phe378 and Glu379 of the LBD from the corresponding crystal structures are shown, colored as **19b** and **24b**; distances shown, between the indicated ligand atoms and Glu379:N of the LBD from the relevant complex structure, are in Å. The overlay is based on superposition of the LBD in the crystal structures of the two complexes.

Table 1. Binding and cell-based functional data of 3-phenyl-2,4-dichloroquinolines.[a]

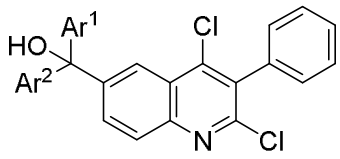

Cmpd #	Ar^1	Ar^2	ThermoFluor® binding to RORγt LBD, K_d (nM)	RORγt cell-based reporter assay IC_{50} (nM) (% inhibition at 6 μM)
1	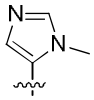	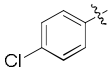	160	260 (101)
2	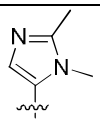	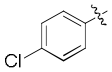	190	600 (106)
3	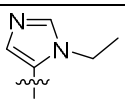	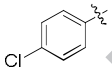	450	820 (101)
4	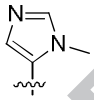	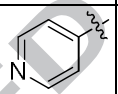	14	50 (105)
5	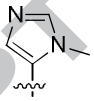	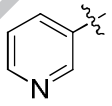	38	140 (103)
6	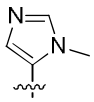	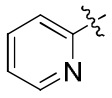	960	1000 (93)
7	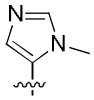	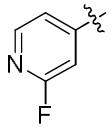	5.3	21 (103)
8		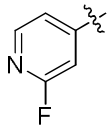	20000	>6,000 (37)

9	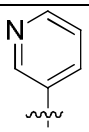	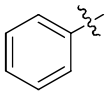	76	130 (100)
10	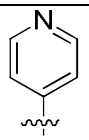	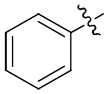	1500	2100 (84)
11	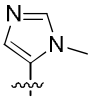	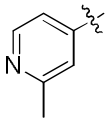	0.60	13 (104)
12	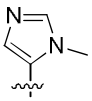	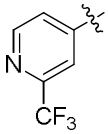	6.4	82 (101)
13	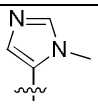	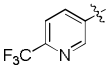	31	180 (100)
14	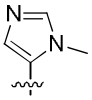	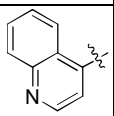	0.50	5.5 (101)
15	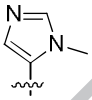	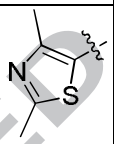	1.1	100 (104)

[a] Compounds in Table 1 were tested as racemic mixtures.

Table 2. Activities of single enantiomers of screening hit **1**.

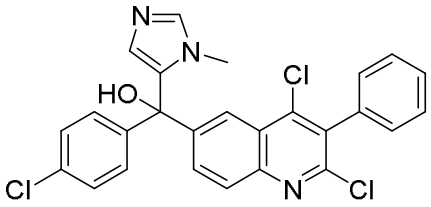

Cmpd #	ThermoFluor® binding to RORγt LBD, K_d (nM)	RORγt cell-based reporter assay IC_{50} (nM) (% inhibition at 6 μM)

1[a]	160	260 (101)
1a[b]	32	220 (100)
1b[b]	5700	~5500 (58)

[a] Racemate.
[b] Single enantiomer, absolute stereochemistry not determined.

Table 3. Binding and cell-based functional data of 2-methoxy-3-(1-pyrazole-benzyl)-4-chloroquinolines.[a]

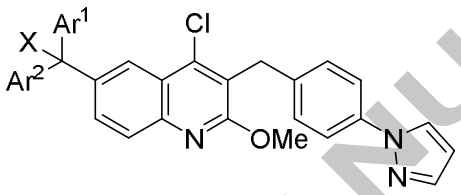

Cmpd #	Ar^1	Ar^2	X	ThermoFluor® binding to RORγt LBD, K_d (nM)	RORγt cell-based reporter assay IC_{50} (nM) (% inhibition at 6 μM)
16a	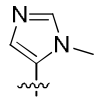	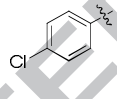	OH	9.2	73 (99)
16b	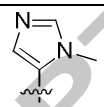	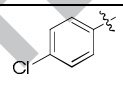	OH	520	670 (87)
17	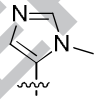	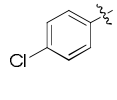	NH_2	110	210 (97)
18	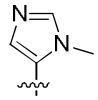	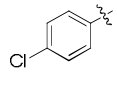	NHMe	280	630 (90)
19a	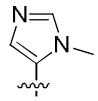	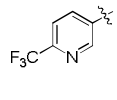	OH	5.0	89 (97)
19b	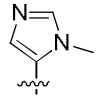	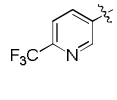	OH	70	170 (99)
20a	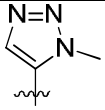	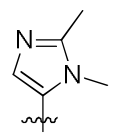	OH	1.2	13 (100)

20b	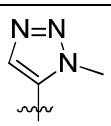	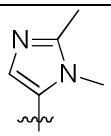	OH	0.38	5.3 (100)
21	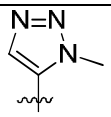	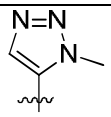	OH	5.0	6.6 (91)
22	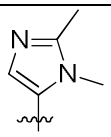	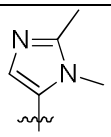	OH	0.27	200 (96)
23a	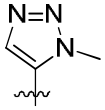	H	OH	69	270 (98)
23b	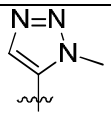	H	OH	91	300 (97)
24a	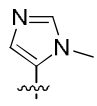	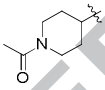	OH	20	46 (100)
24b	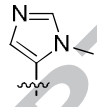	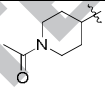	OH	33	59 (107)
25a	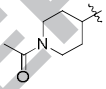	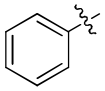	OH	3.6	24 (100)
25b	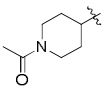	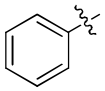	OH	77	140 (103)

[a] All chiral compounds are single enantiomers. Absolute stereochemistry is unknown unless specifically noted in the text.

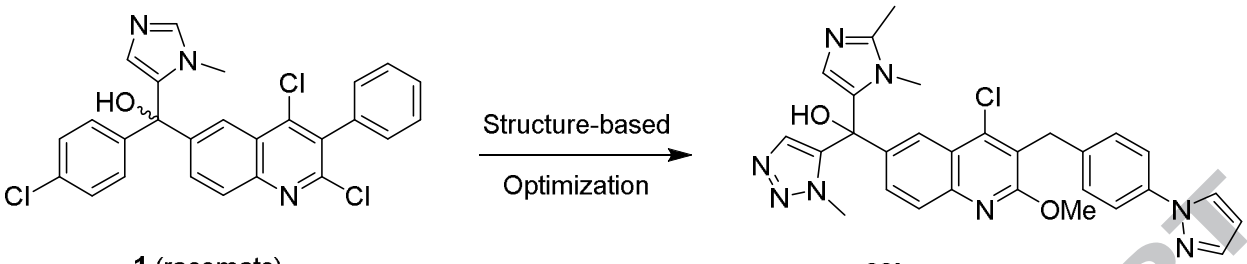

1 (racemate)
Binding K_d 160 nM
Cell reporter IC_{50} 260 nM

20b (single enantiomer)
Binding K_d 0.38 nM
Cell reporter IC_{50} 5.3 nM